JOURNAL OF MECHANICAL ENGINEERING AND SCIENCES
ISSN: 2289-4659 e-ISSN: 2231-8380
VOLUME 19, ISSUE 1, 2025, 10440 - 10454
DOI: https://doi.org/10.15282/jmes.19.1.2025.3.0820

RESEARCH ARTICLE

Effect of after burn cooling on temperature and damage of human skin: A finite element approach

A. M. M. Mukaddes[1]*, M. Sannyal[2] , M. Junaid[3]

[1] Department of Industrial and Production Engineering, Shahjalal University of Science and Technology, Sylhet-3114, Bangladesh
Phone: + 8801777891684

[2] Department of Information, Gildan, Gulshan-2, Dhaka-1000, Bangladesh

[3] Department of Mechanical Engineering, Shahjalal University of Science and Technology, Sylhet-3114, Bangladesh

ABSTRACT - Burn injuries are a significant health concern, requiring immediate and effective intervention to minimize tissue damage. Experimental measurement of temperature variations in live tissues is challenging, making numerical simulations, such as the finite element method, essential for studying skin temperature distribution and evaluating cooling strategies. This study aims to develop a finite element model to simulate the thermal response of human skin during and after heat exposure and to compare the effectiveness of various first-aid cooling methods. A 2D finite element code was developed in C programming language, with key assumptions including negligible metabolic heat generation and perfect thermal contact between the skin and a hot disk at 90°C for 15 seconds. Post-burn cooling strategies analyzed include ambient air, water immersion, flowing water jets, ice, and cryogenic spray. The results demonstrate that ice cooling was the most effective, reducing epidermal temperature to 0 °C within 32 seconds, though it poses risks of hypothermia. Water jets using forced convection were the second most efficient, lowering tissue temperature below critical damage thresholds 35% faster than water immersion. Cryogenic spray cooling, despite its rapid localized effect, was less effective due to limited tissue coverage. The finite element analysis provided quantitative insights into temperature reductions across skin layers and calculated burn damage integrals over time for each method. This study highlights the critical role of finite element modeling in understanding post-burn treatment dynamics. The findings provide guidance for selecting optimal cooling strategies and serve as a basis for developing advanced cooling devices and refining first-aid protocols.

ARTICLE HISTORY

Received	:	31st Mar. 2024
Revised	:	18th Nov. 2024
Accepted	:	03rd Mar. 2025
Published	:	30th Mar. 2025

KEYWORDS

Skin burn
Finite element
Afterburn cooling
Damage integral

1. INTRODUCTION

The skin, the body's largest organ, plays a multifaceted role, functioning as a protective barrier, sensory interface for temperature and pain, and a critical component of thermoregulation. Its impermeability to environmental chemicals and tissue fluids also highlights its vital role in safeguarding the body's internal systems. However, one of the most common and severe traumas affecting the skin is burns, leading to significant morbidity and mortality. Burn injuries are responsible for approximately 180,000 deaths annually, primarily in low- and middle-income countries [1]. Additionally, non-fatal burns result in prolonged suffering and long-term disability. Burns frequently occur in domestic and workplace environments, with fire and explosions being the most common causes, particularly among children and the elderly [1]. The National Fire Protection Association reports that nearly 30% of fires begin in homes, further elevating the risk of burns in such environments [2].

Burns are caused by the transfer of excess thermal energy to the skin through various means such as fire, explosions, radiation, electrical sources, chemicals, and hot objects or fluids. This excess energy raises the temperature of the skin above its damage threshold, resulting in irreversible tissue damage. Thermal burns, which occur due to exposure to flames, hot solids, or liquids above body temperature, are a particular focus of this research. When the skin's temperature surpasses the burn threshold, irreversible damage begins, impacting the skin's structure and function [3]. Several factors contribute to the severity of burns, including the thermal properties of the skin, the nature of the heat source, exposure duration, temperature, and heat flux. Structurally, the skin consists of three layers: the outer epidermis, which provides primary protection; the dermis, a fibrous layer that strengthens the epidermis; and the subcutaneous layer, which insulates and nourishes the other layers [4]. Burns are classified into degrees based on their severity, ranging from minor first-degree burns affecting only the epidermis, to severe third-degree burns that extend through the dermis and subcutaneous layers, potentially damaging underlying tissues [5].

While the damage from burns is irreversible, the extent of further harm can be minimized by appropriate first-aid measures, with cooling being the most widely accepted and ancient method for mitigating burn severity. From ancient Egypt to modern medical practices, cooling has been used to reduce burn severity and relieve pain. Common cooling

*CORRESPONDING AUTHOR | A. M. M. Mukaddes | ✉ mukaddes-ipe@sust.edu

methods include cold water immersion and cold air convection. Studies have shown that immersing a burn in cold water significantly decreases skin temperature and limits tissue damage [6]. Research by Klavuhn and Green [7], as well as Cao et al. [8], explored the effects of contact cooling with ice or cooling pads, highlighting the effectiveness of sapphire cooling in reducing heat in the epidermis for short pulse duration. Other studies, such as those conducted by Smakulski [9], have emphasized the importance of cryogenic spray cooling, particularly in high heat flux environments, capable of managing fluxes up to 300 W/cm². These methods have been shown to be effective, but limitations remain in their practical application. Experimental studies have consistently demonstrated that cooling can decrease pain, reduce tissue damage, and lower mortality rates. Cold water, in particular, has been shown to be highly effective in relieving pain and preventing burn propagation [10, 11].

Immediate first aid following a burn injury is crucial for improving recovery outcomes. The World Health Organization (WHO) recommends the use of running water as the most effective first-aid treatment for burns [1]. Mukaddes and Junaid [6] provided key insights into optimizing running water as a cooling method, demonstrating that water at 15 °C cools burn wounds 20–30% faster than immersion in water at the same temperature. However, their study did not consider the effects of different degrees of burns. Measuring temperature variations in live tissues presents a significant challenge in experimental settings. Numerical simulations, such as those utilizing the finite element method, offer an alternative for studying temperature distribution across skin layers, which is difficult to achieve through vivo experiments [12, 13]. Traditional one-dimensional analysis is limited in its ability to capture the full extent of temperature variation in tissue, and boundary conditions for heat transfer during cooling cannot be accurately applied in such models. This study addresses these limitations by employing the finite element method in a 2-D programming code, designed to simulate the thermal response of the human body, developed in C programming language. Our calculations were validated against analytical data.

This research aims to develop a mathematical model to simulate the thermal response of human skin to burns, followed by different cooling methods. The model focuses on the heating phase, simulating contact with a hot surface, and the cooling phase, comparing various methods such as ambient air cooling, water bath immersion, ice contact, and cryogenic spray cooling. By analyzing the progression of skin damage under different cooling scenarios, this study seeks to identify the most effective first-aid cooling methods for burns. The outcomes of this research will provide valuable insights for both medical practitioners and researchers in the field of burn treatment and cooling technology development, enabling better strategies for minimizing burn severity and enhancing future designs for burn care products and medical devices.

2. MATERIALS AND METHODS

2.1 Mathematical Model

The human skin can be conceptualized as comprising three distinct regions, each characterized by unique material properties. These regions include the outermost layer, known as the epidermis, situated above the dermis, and the fat layer. A schematic diagram in Figure 1 illustrates the skin model, where Ω_1 (0.008 mm × 7 mm) represents the epidermis, Ω_2 (2.08 mm × 7 mm) denotes the dermis, and Ω_3 (10mm×7mm) corresponds to the fat region [14]. Additionally, the length of Γ_4 is 1.5 mm, and Γ_5 is 8 mm, with Γ_6 positioned at the central point of the domain.

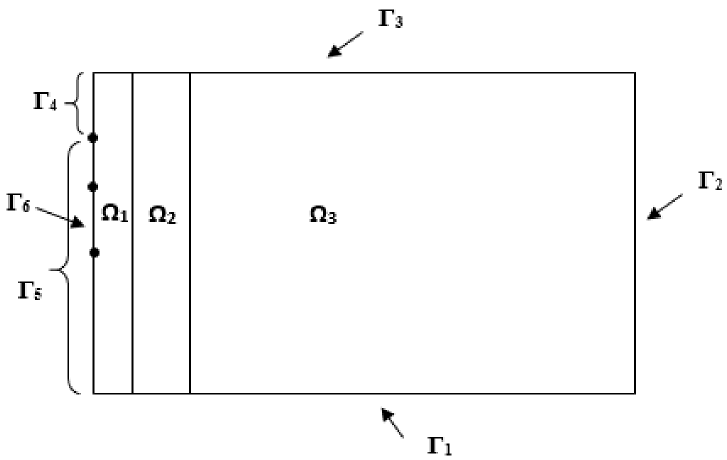

Figure 1. Schematic diagram of the human skin model

2.2 Governing Equation with Boundary Conditions

The transient temperature distribution within the skin is determined by the well-known Penne's Bioheat equation [15], which is expressed as follows:

$$k\frac{\partial^2 T}{\partial x^2}+\frac{\partial^2 T}{\partial y^2}+\omega_b\rho_b c_b(T_a-T)+Q_m+Q_r=\rho c\frac{\partial T}{\partial t} \quad (1)$$

In this study, the variables ρ, c, and k represent the density, specific heat, and thermal conductivity of the tissue, respectively. The symbols c_b and ρ_b refer to the specific heat and density of blood, while ω_b signifies the blood perfusion. Additionally, T_a represents the arterial temperature, and T denotes the unknown skin tissue temperature. The term Q_m corresponds to the metabolic heat generation, and Q_r represents the heat source resulting from spatial heating over time, t. In the present study, it is assumed that the metabolic rate in the skin is nearly negligible, setting Q_m = 0. Furthermore, no external heating is applied in our investigation, leading to Q_r = 0. Then Eq. (1) becomes

$$k\frac{\partial^2 T}{\partial x^2}+\frac{\partial^2 T}{\partial y^2}+\omega_b\rho_b c_b(T_a-T)=\rho c\frac{\partial T}{\partial t} \tag{2}$$

The boundary conditions used in this study are listed below.

$$\begin{aligned}
k\frac{\partial T}{\partial x}\eta_x+\frac{\partial T}{\partial y}\eta_y &= 0 \quad \text{on} \quad \Gamma_1 \text{ and } \Gamma_3\\
T &= T_c \quad \text{on} \quad \Gamma_2 \text{ (body core temperature)}\\
T &= T_d \quad \text{on} \quad \Gamma_5 \text{ (for heating with disk}\\
k\frac{\partial T}{\partial x}\eta_x+k\frac{\partial T}{\partial y}\eta_y &= h(T_f-T) \text{ on } \Gamma_4 \text{ (for cooling)}\\
T &= T_{ice} \quad \text{on} \quad \Gamma_5 \text{ (for ice cooling)}
\end{aligned} \tag{3}$$

In this context, T_c represents the core temperature of the body, while T_d denotes the temperature of the heating disk. The ambient heat transfer coefficient is denoted as h, and T_f represents the temperature of the cooling fluid. All the boundary conditions are used at the same time but from case to case.

2.3 Cryogenic Cooling Conditions

Cryogenic spray finds extensive application in cryoablation, a surgical method employing freezing temperatures to treat biological tissues. Various freezing agents are employed in cryogenic sprays, including ice (0 °C), ice-salt mixture (-20 °C), freon (-29.80 °C to -40 °C), and liquid nitrogen (-196 °C) [16]. The notably low temperatures of cryogenic spray, ranging from 0 °C to near absolute zero, provide substantial benefits for cooling human skin. In laser therapies, cryogenic spray cooling is utilized to mitigate the risk of damage to the epidermis and dermis, thereby minimizing adverse thermal effects.

2.4 Burn Quantification

Numerous mathematical models have been proposed to quantify burn severity, with one of the most notable being Henriques' model which demonstrated that skin damage follows the dynamics of a chemical rate process. Henriques introduced the use of the Arrhenius rate equation to characterize the rate of tissue injury based on temperature and exposure time. The Henriques burn integral, derived from this equation, is utilized in the present study to quantify burn damage accurately [17]. The expression of the equation is as follows:

$$\Omega=\int\rho c\int_0^t P\,exp\left(-\frac{\Delta E}{RT}\right)dt \tag{4}$$

where, Ω is the damage index, P is the pre-exponential factor $[S^{-1}]$, ΔE is the activation energy [J mole^{-1}], R is the molar gas constant (8.3144621 Jkg^{-1}mole^{-1}), and T is the skin temperature ($in\ Kelvin$). The damage index, Ω is a measure of the injury. Later, other researchers agreed to use Henrique's burn integral but wanted a different combination of Pre-exponential factor and activation energy [18].

2.5 Finite Element Discretization

Using the Weighted Residual Method [19], linear system of equations was obtained from the Eq. (4) using the following steps.

$$\int_\Omega[w\rho c\frac{\partial T}{\partial t}-w(k\frac{\partial^2 T}{\partial x^2}+k\frac{\partial^2 T}{\partial y^2})-CwT_a+CwT]dxdy=0 \tag{5}$$

where, $C=w_b\rho_b c_b$ and w is the weight function. It is known that,

$$\int_\Omega -w\frac{\partial}{\partial x}\left(k\frac{\partial T}{\partial x}\right)dxdy=\int_\Omega k\frac{\partial w}{\partial x}\frac{\partial T}{\partial x}dxdy-\oint_\Gamma wk\frac{\partial T}{\partial x}\eta_x ds \tag{6}$$

$$\int_\Omega -w\frac{\partial}{\partial y}\left(k\frac{\partial T}{\partial y}\right)dxdy=\int_\Omega k\frac{\partial w}{\partial y}\frac{\partial T}{\partial y}dxdy-\oint_\Gamma wk\frac{\partial T}{\partial y}\eta_y ds \tag{7}$$

Now the Eq. (5) is reduced to,

$$0=\int_{\Omega}\left[w\rho c\frac{\partial T}{\partial t}+k\frac{\partial w}{\partial x}\frac{\partial T}{\partial x}+k\frac{\partial w}{\partial y}\frac{\partial T}{\partial y}+CwT-wf\right]dxdy-w\oint_{\Gamma}\left(k\frac{\partial T}{\partial x}\eta_x+k\frac{\partial T}{\partial y}\eta_y\right)ds \tag{8}$$

Here, w is the weighted function. For convective boundary as $k\frac{\partial T}{\partial x}\eta_x+k\frac{\partial T}{\partial y}\eta_y=-\mathrm{h}(T-T_0)$ the boundary integral modified as following to account for the convective heat transfer term. Here, h is the convective heat transfer coefficient, T_o is the ambient temperature [20]:

$$0=\int_{\Omega}[w\rho c\frac{\partial T}{\partial t}+k\frac{\partial w}{\partial x}\frac{\partial T}{\partial x}+k\frac{\partial w}{\partial y}\frac{\partial T}{\partial y}+CwT-wf]dxdy\ -w\oint_{\Gamma}[h(T-T_o)]ds \tag{9}$$

Using a quadratic approximation function as $T_h^e(x)=\sum_{j=1}^{e}\varphi_j^e(x)\,T_j^e$, the finite element model of the governing differential equation is thus derived as [20]:

$$\begin{aligned}0=&\int_{\Omega}\rho c\psi_i^e\psi_j^e\frac{\partial T_j^e}{\partial t}dxdy\ +\int_{\Omega^e}^{e}\left[\left\{k\frac{\partial\psi_i^e}{\partial x}\frac{\partial\psi_j^e}{\partial x}+k\frac{\partial\psi_i^e}{\partial y}\frac{\partial\psi_j^e}{\partial y}+C\psi_i^e\psi_j^e\right\}dxdy+\oint_{\Gamma}^{e}h\psi_i^e\psi_j^e ds\right]T_j^e\\&-\int_{\Omega}^{e}f\psi_i^e dxdy-\oint_{\Gamma}^{e}\psi_i^e hT_0 ds\end{aligned} \tag{10}$$

Finally, the finite element model of the governing differential equation is derived as following [20]:

$$\begin{aligned}0=\sum_{j=1}^{n}\Bigg\{&\int_{\Omega}\rho c\psi_i^e\psi_j^e\frac{\partial T_j^e}{\partial t}dxdy+\int_{\Omega}\left[\left\{k\frac{\partial\psi_i^e}{\partial x}\frac{\partial\psi_j^e}{\partial x}+k\frac{\partial\psi_i^e}{\partial y}\frac{\partial\psi_j^e}{\partial y}+C\psi_i^e\psi_j^e\right\}dxdy+\oint_{\Gamma}h\psi_i^e\psi_j^e ds\right]T_j^e\\&-\ \int_{\Omega}f\psi_i^e dxdy-\oint_{\Gamma}\psi_i^e hT_o ds\Bigg\}\end{aligned} \tag{11}$$

The simplified form of Eq. (11) is written as:

$$0=\sum\nolimits_{j=1}^{n}\{C_{ij}^e\dot{T}_{ij}^e+[K_{ij}^e+H_{ij}^e]T_{ij}^e-q_j^e-Q_j^e\} \tag{12}$$

Here, $C_{ij}^e=\int_{\Omega}\rho c\psi_i^e\,\psi_j^e$; $K_{ij}^e=\int_{\Omega}k\frac{\partial\psi_i^e}{\partial x}\frac{\partial\psi_j^e}{\partial x}+k\frac{\partial\psi_i^e}{\partial y}\frac{\partial\psi_j^e}{\partial y}+C\psi_i^e\psi_j^e$; $H_{ij}^e=h\oint_{\Gamma}\psi_i^e\psi_j^e$; $q_i^e=f\int_{\Omega}\psi_i^e dxdy$; $Q_i^e=\oint_{\Gamma}h_0T_0\psi_i^e ds$

In matrix notation Eq. (12) can be expressed as [20]:

$$[C]\{\dot{T}\}+[K]\{T\}=\{q\}+\{Q\} \tag{13}$$

where, C is the capacitance matrix, K is the heat conductive matrix with convection term in the boundary and T is unknown temperature, and others are known vectors.

A simple time integration scheme for Eq. (13) was derived. In that case, the matrix differential equation can be discretized on time as [20]:

$$C\frac{T^{n+1}-T^n}{\Delta t}+\alpha KT^{n+1}+(1-\alpha)KT^n\ =Q+q \tag{14}$$

where, T^{n+1} and T^n are the vectors of unknown nodal values at times $n\Delta t$ and $(n+1)\Delta t$ respectively, α is the weighting factor which must be chosen in the interval between 0 and 1. Equation (12) the standard approximation for time derivative was used as $\dot{T}=\frac{T^{n+1}-T^n}{\Delta t}$.

When the value of α is considered 0.5, the process is called the popular Crank-Nicolson method [21]. The discretized Eq. (14) can be written as [20]:

$$\left(C\frac{1}{\Delta T}+\alpha K\right)T^{n+1}=\left[C\frac{1}{\Delta T}-(1-\alpha)K\right]T^n+q+Q \tag{15}$$

At first Eq. (9) was solved using an iterative procedure. The initial temperature is known and then the temperature of the next step can be calculated from the solution of Eq. (15).

3. RESULTS AND DISCUSSION

The numerical solution of the study is divided into two distinct stages: the heating phase and the cooling phase. The heating phase occurs from t = 0 second to t = 15 seconds, during which the skin is exposed to thermal energy from a heated disk. Following this, the cooling phase begins immediately after the heating phase, during which various cooling strategies are implemented to evaluate their effectiveness. The cooling methods considered in this study include the following cases:

Case 1 involves natural convection cooling by air, with a heat transfer coefficient, h of 7 W/ (m^2 °C) and an ambient temperature, T of 25 °C. Case 2 focuses on convection cooling by water, which is further divided into two sub-cases. In Case 2.2, the skin is immersed in a water bath with a heat transfer coefficient, h_f of 500 W/ (m^2 °C) and a water temperature, T_f of 10 °C. In Case 2.3, cooling is achieved using flushed water, with a higher h_f of 1000 W/ (m^2 °C) and the same water temperature of 10 °C. Case 3 examines contact cooling by ice, while Case 4 evaluates cooling through the application of a cryogenic spray. The results demonstrate that increasing the h and the thermal conductivity of the cooling medium significantly enhances the rate of heat transfer, thereby improving the cooling efficiency. The thermal properties and other control values utilized in this study are summarized in Table 1.

Table 1. Thermal properties and control values [6, 9, 21-23]

Parameter	Symbol	Value
Thermal conductivity:		
Epidermis		0.255 W/m °C
Dermis	k	0.523 W/m °C
Sub-Cutaneous tissue		0.167 W/m °C
Blood Perfusion:		
Epidermis		0.0 ml/s/ml
Dermis	ω_b	0.00125 ml/s/ml
Sub-Cutaneous tissue		0.00125 ml/s/ml
Density		
Epidermis		1200 kg/m^3
Dermis	ρ	1200 kg/m^3
Sub-Cutaneous tissue		1000 kg/m^3
Specific heat		
Epidermis		3598 Jkg^{-1} °C^{-1}
Dermis	C	3222 Jkg^{-1} °C^{-1}
Sub-Cutaneous tissue		2760 Jkg^{-1} °C^{-1}
Density of Blood	ρ_b	1100 kg/m^3
Specific heat of blood	C_b	3300 Jkg^{-10}C^{-1}
Temperature of the artery	T_a	37 °C
Initial Temperature	$T_{initial}$	34 °C
Heat convection coefficient		
Natural Convection to air	h_o	7 W/m^2 °C
Water Bath	h_f	500 W/m^2 °C
Cooled waterjet	h_f	1000 W/m^2 °C
Cryogenic Cooling	h_c	2200 W/m^2 °C
Temperature of the Cooler		
Ambient Air	T_o	25 °C
Water bath and Cooled water jet	T_f	10 °C
ICE	T_{ice}	0 °C
Freezing Element (Cryogenic Cooling)	T_c	-6 °C
Pre exponential factor, P	P	7.39×10^{39} [1/s]
Activation Energy, ΔE	ΔE	2.577×10^5 Jkg^{-1}k^{-1}
Molar Gas Constant, R	R	8.314×10^3 JKmol^{-1}K^{-1}

3.1 Model Validation

The two-dimensional finite element model of bio-heat equation was validated with the analytical and other numerical results by the authors in [20]. The numerical results of the present code show the similar pattern with the analytical and other simulation results.

3.2 Skin Heating

In this investigation, the skin undergoes heating using a hot disk at a temperature of 90 °C for a duration of 15 seconds. It is assumed that there is perfect thermal contact between the heating disk and the skin surface throughout the process, resulting in equal temperatures, T for both the skin and the heating disk from the initial time (t = 0 second) to the endpoint (t = 15 seconds). The resulting skin temperature after 15 seconds of heating is depicted in Figure 2(a), revealing a maximum temperature of 90 °C at the skin surface in direct contact with the heating disk. However, lower temperatures are observed in other areas of the skin surface due to exposure to the surrounding environment. The isolines in Figure 2(a) indicates the damage index, with values of 0.53, 1, and 10000 chosen to represent first, second, and third-degree burn contours, respectively [22]. Figure 2(b) shows that within the first 15 seconds, tissue faces up-to second degree burn near the skin surface. The skin's surface area in direct contact with the ambient air exhibits reduced thermal damage, with specific regions remaining unaffected. This is due to the absence of direct contact with a heated source and the dissipation of heat to the surroundings via convective heat transfer.

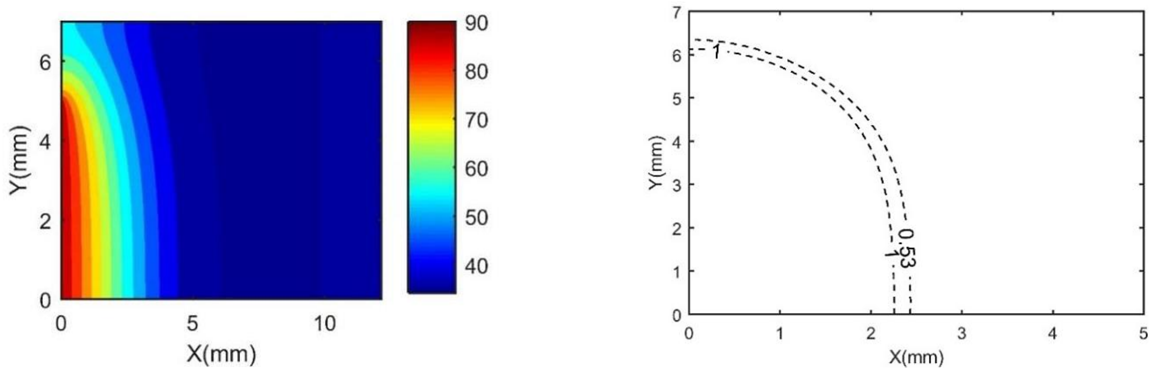

(a) (b)

Figure 2. Tissue temperature (a) and damage index (b) after 15 seconds

3.3 Convection Cooling

In the process of convection cooling, heated skin tissue is exposed to either air or cool water for the purpose of cooling. When the skin comes into contact with the surrounding air, this cooling method is referred to as natural cooling by the ambient air. In Figure 3(a)-(c), the temperature distribution resulting from after burn cooling in the ambient air (25 °C) is illustrated after 20, 35, and 50 seconds, respectively. After a 20-second period as illustrated in Figure 3(a), natural cooling reduces the epidermal maximum temperature from 90 °C to 80 °C. Continued cooling leads to a further decrease, with the epidermal temperature reaching 55 °C at 35 seconds and 45 °C at 50 seconds.

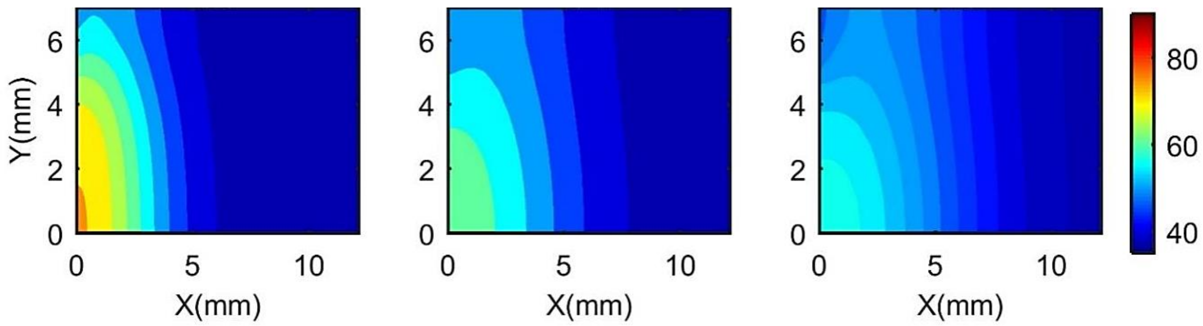

(a) (b) (c)

Figure 3. Cooling with ambient air: (a) 20 seconds, (b) 35 seconds, and (c) 50 seconds

During the 35-second and 50-second intervals, the dermis registers higher temperatures than the epidermis. This phenomenon arises because the epidermis is more susceptible to cooling than the dermis. The temperature loss due to cooling is more pronounced in the epidermis compared to the dermis. Consequently, after 35 seconds, the epidermis temperature is 55 °C, while the dermis temperature is 60 °C. A similar trend is observed after 50 seconds of heating.

Figure 4 illustrates the temperature distribution over time under two cooling methods: natural cooling using a water bath and forced convection via a cooled water jet. Specifically, Figures 4(a)-(c) show the temperature decrease after intervals of 20, 35, and 50 seconds for natural cooling. In contrast, Figures 4(d)-(f) depict the corresponding temperature drops under forced convection at the same points. However, as depicted in Figure 4, the rate of temperature decline is more pronounced in the forced convection cooling compared to the natural convection. After 20 seconds of cooling in a water bath, the maximum temperature reaches 65 °C for the forced convection, in contrast to 80 °C for natural convection. Natural convection cooling further reduces the temperature to 55 °C and 45 °C after 35 seconds and 50 seconds of cooling in the water bath, respectively. In the case of flush water cooling, the temperature drops to 35 °C after 35 seconds and to

30 °C after 50 seconds. It is essential to emphasize that biological tissue does not undergo cell destruction until it exceeds a certain damage threshold. This threshold is a critical parameter in evaluating the efficiency of cooling techniques. A smaller proportion of the area surpassing the damage threshold indicates less harm to the skin, signifying a more effective cooling approach. Figure 5(a) depicts the percentage of the area exceeding the threshold value, while Figures 5(b) and 5(c) concentrate on the dermis and fat layers, respectively. The graph in Figure 6(a) shows that all cells in the epidermis exceed the damaged threshold values during the heating process. The impact of cooling becomes noticeable after nearly 18 seconds of forced cooling using natural air and water. In contrast, natural cooling through air or cool water (Cases 1.1 and 2.1) does not exhibit a significant effect until around the 50-second mark. However, forced cooling demonstrates a considerable impact, resulting in a rapid reduction in skin temperature.

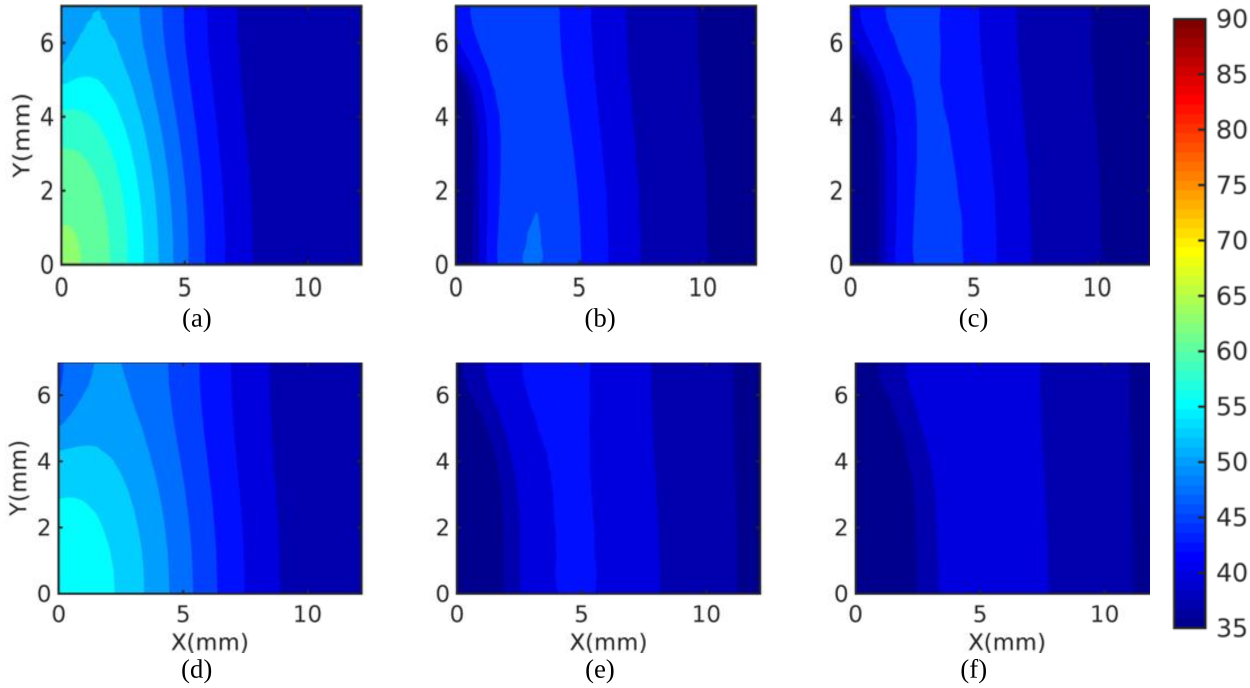

Figure 4. Force convection cooling with water after: (a) t=20s, h=500 W/m^2K, (b) t=35s, h=500 W/m^2K, (c) t=50s, h=500 W/m^2K, (d) t=20s, h=1000 W/m^2K, (e) t=35s, h=1000 W/m^2K and (f) t=50s, h=1000W/m^2K

In Case 2.1, it takes approximately 40 seconds to lower the temperature of the entire domain below the threshold value. Both Case 2.2 and Case 2.3 achieve this in about 35 seconds. The most favorable outcome is observed in cooling through flush water at 10 °C, where it takes around 18 seconds to decrease half of the cell temperature below the threshold value and approximately 32 seconds for all cells. Consequently, the current experimental setup indicates that flush water cooling is more efficient in rapidly reducing tissue temperature beyond the threshold value compared to cooling air circulation (Case 1.1) and skin immersion in water (Case 2.1 and Case 2.2).

In Figure 5, a comparable situation is depicted, illustrating the proportion of the area surpassing the damage threshold temperature with various cooling methods. The outcomes for the epidermis, dermis, and fat are presented in Figure 5(a), Figures 5(b), and 5(c), respectively. Following 15 seconds of heating, the entire epidermis experienced temperature elevation beyond the damage threshold, subsequently leading to the dermis surpassing the damage threshold value, as evidenced in Figures 5(a) and 5(b). The fat also exceeded the damage threshold temperature during this period. The situation persisted for 50 seconds with convection cooling to the ambient air, but the accumulation area began decreasing when the skin was subjected to the water cooling, either through flushing or immersion. Flush water cooling took approximately 32 seconds to bring the entire epidermis temperature below the damage threshold, while water bath cooling required about 35 seconds. Similarly, for the dermis, flush water cooling took 40 seconds, whereas water bath cooling needed nearly 45 seconds. Although both the epidermis and dermis layers entirely surpassed the damage threshold, only 20% of the fat cells exceeded that value after 15 seconds of heating.

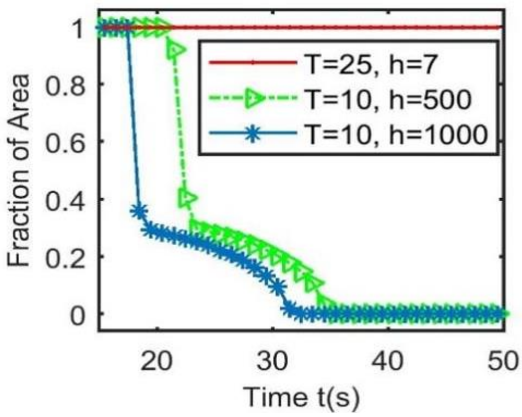

(a)

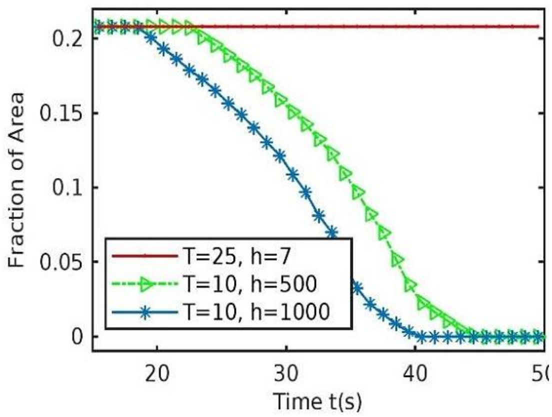

(b)

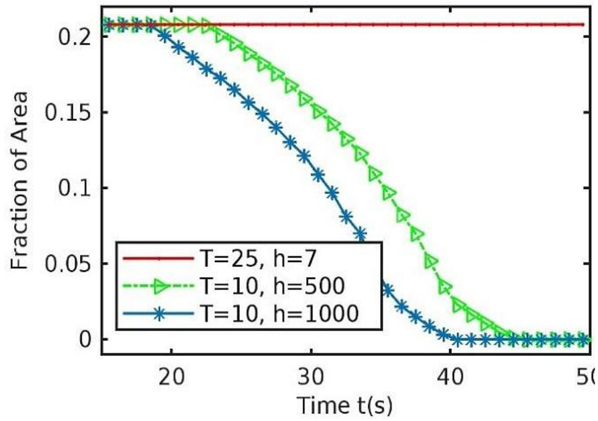

(c)

Figure 5. Fraction of tissue area over 42 °C temperature during convection cooling: (a) epidermis, (b) dermis and (c) fat

Flush water cooling efficiently reduces the temperature, reaching below the damage threshold for all skin layers. It took about 40 seconds for flush water cooling to achieve this for the skin, while water immersion cooling required approximately 45 seconds. The heat transfer coefficient of flush water (1000 W/m²K) is significantly higher than that of still water (500 W/m²K), resulting in a faster cooling rate for flush water compared to still water. Figure 6 illustrates the impact of cooling on first-degree burns. In Figure 6(a), the percentage of epidermal areas affected by first-degree burns is presented. Figure 6(b) displays the dermal area affected, while Figure 6(c) represents the fat area. In Cases 1.1 and 2.1 within the 50 seconds timeframe, all epidermal cells experience first-degree burns, with approximately 88% of dermal cells affected and 12% of fat cells impacted. Cases 2.3 and 2.2 exhibit similar outcomes, with 85% cell damage to the epidermis, 80% to the dermal region, and 5% and 4% cell damage to the fat region, respectively. Notably, cooling through flush water in Case 2.3 yields the most favorable results, causing destruction to 82% of epidermal cells, 78% of dermal cells, and only 3.8% of fat cells significantly lower than the other cases. In Figure 7, the impact of cooling on second-degree burns is illustrated. Figure 7(a) depicts the proportion of the epidermal area affected by second-degree burns. Additionally, Figure 7(b) presents the first-degree burn's influence on the dermal area, while Figure 7(c) highlights the fat area. Analysis of second-degree burns reveals that Case 2.3 demonstrates the most favourable outcomes among all cases, followed by Case 1.1, Case 2.2, and Case 2.3. Conversely, Cases 1.1 and 2.1 yield the most detrimental results, causing nearly 96% cell damage to the epidermal region, 87% to the dermal region, and 7% to the fat. Hence, it is evident that Cases 1.1 and 2.1 lead to more severe consequences than the other scenarios. The comparison indicates that natural convection is considerably less effective than forced convection. Notably, employing forced convection with cold water proves to be the most efficient cooling method when compared to alternative approaches.

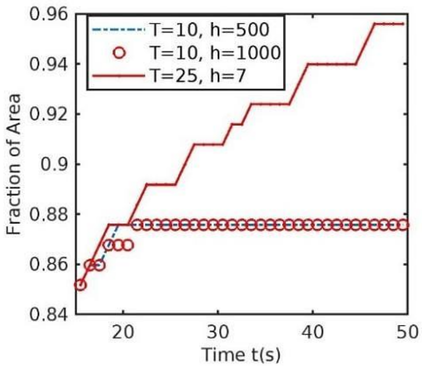

(a)

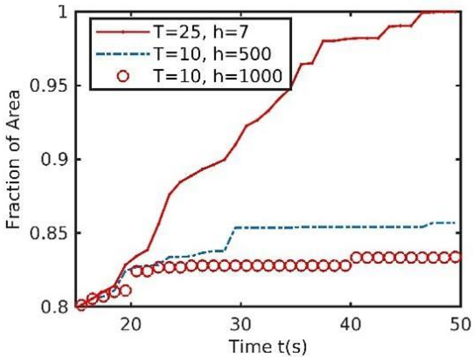

(b)

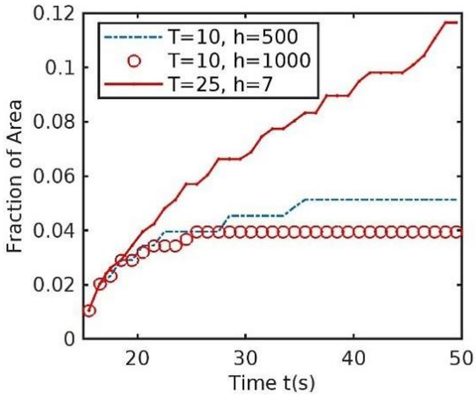

(c)

Figure 6. Fraction of tissue area affected by first degree burn during convection cooling: (a) epidermis (b) dermis (c) fat

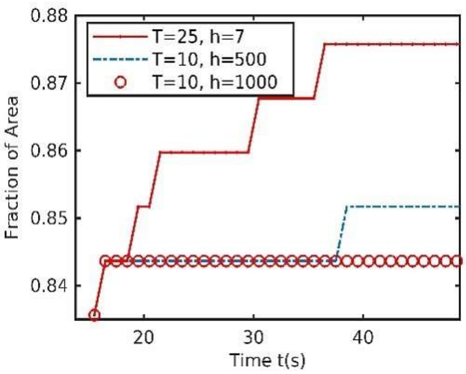

(a)

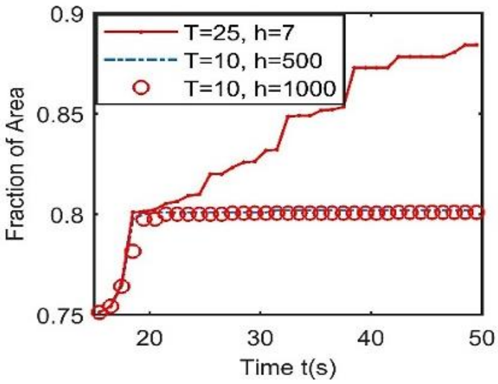

(b)

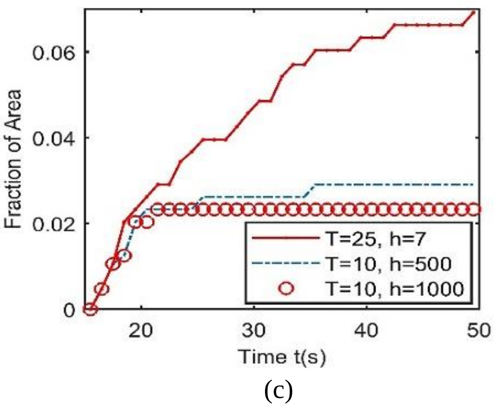

(c)

Figure 7. Fraction of tissue area affected by second-degree burn during convection cooling: (a) Epidermis (b) Dermis (c) Fat

3.4 Ice Cooling

Another method of first aid for treating burns involves the application of ice for cooling purposes, wherein the ice makes direct contact with the burned tissue. The low temperature of the ice (0 °C) facilitates a swift cooling process, leading to a rapid decrease in the intensity of the burn [16]. This section presents an analysis of the temperature and damage profile when subjected to ice cooling. In Figure 8, the temperature profiles over different time intervals are presented. Figures 8(a), 8(b), and 8(c) demonstrate that following the application of ice cooling for durations of 20, 35, and 50 seconds, the epidermal temperature remains within a relatively lower range, whereas an elevated temperature persists in the dermal layer. However, with the passage of time, the dermis temperature undergoes a significant drop. After 20 seconds, the maximum recorded temperature exceeds 50 °C, but it diminishes to 30 °C after 50 seconds. In each case, fat temperature remains relatively stable, with cooling having a noticeably reduced impact on fat compared to core body temperature. This difference arises from fat's lower thermal conductivity, which slows heat transfer.

In Figure 9 the depicted region illustrates the extent to which it surpassed the temperature threshold, causing damage to various skin layers. Following a 15-second exposure to heat, nearly 82% of the dermis and approximately 18% of the fat layer exceeded the critical temperature for damage. As the cooling process initiates, the affected area diminishes. Specifically, the epidermal region returns to a temperature below the damage threshold after around 28 seconds, achieving 0% overheating. The dermal layer requires roughly 34 seconds for complete cooling, while the fat layer exhibits a longer duration, taking about 36 seconds. These findings suggest that the fat layer displays a lower sensitivity to cooling compared to the other skin layers.

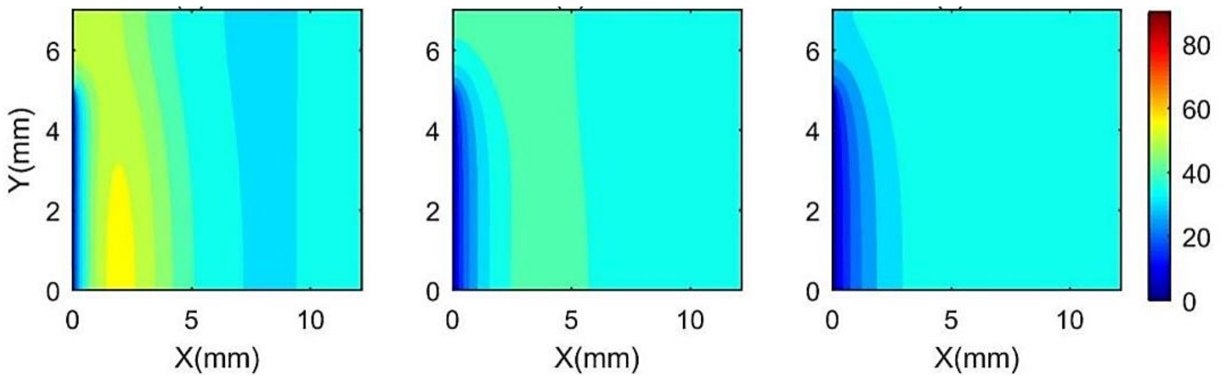

(a) (b) (c)

Figure 8. Afterburn Tissue temperature due to ICE cooling after: (a) 20 seconds, (b) 35 seconds and 50 seconds

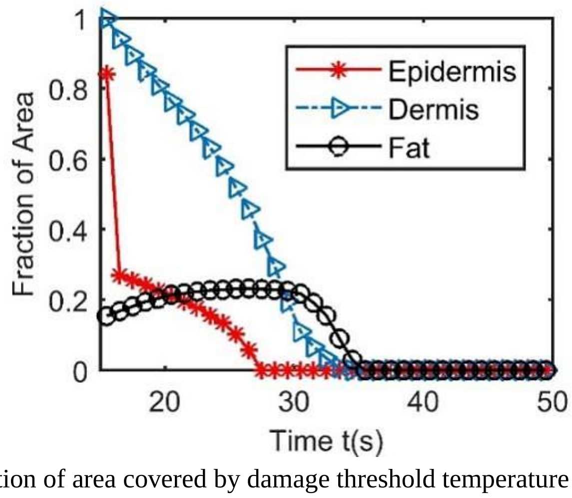

Figure 9. Fraction of area covered by damage threshold temperature during ice cooling

In Figure 10, the impact of burns on different skin layers is illustrated. Subfigures 10(a)-(c) depict the outcomes for the epidermis, dermis, and fat, respectively. Following the application of heat, initial-degree burns affected approximately 82% of the epidermis, 76% of the dermis, and 1% of the fat. These first-degree burns expanded, covering nearly 86% of the epidermis within 25 seconds. Despite ICE cooling limiting further damage to the epidermis after 25 seconds, the dermis and fat continued to experience spreading damage. Beyond the 50-second mark, almost 88% of the dermis and approximately 3.8% of the fat succumbed to first-degree burns. Notably, after 50 seconds, first-degree burns affected 86% of the epidermis, with the dermis surpassing the epidermis at almost 88% in terms of percentage. This disparity arises from the dermis being less responsive to cooling compared to the epidermis. Second-degree burns, starting at 79%

of the base epidermal area after heating, escalated to cover 82% of the epidermis after 50 seconds. Simultaneously, the dermis saw an increase from 71% to 78%, while the fat rose from 1% to 2%, affected by second-degree burns.

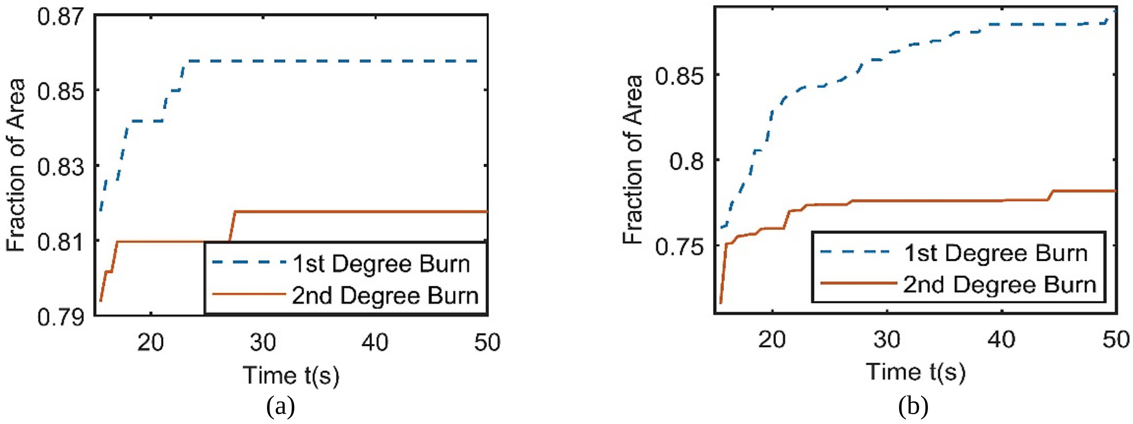

Figure 10. Burn affected area subject to ice cooling for: (a) epidermis, (b) dermis, and (c) fat

3.5 Cryogenic Cooling

The temperature profiles shown in Figures 11(a)-(c) demonstrate the impact of cryogenic spray at successive time intervals of 20, 35, and 50 seconds, respectively. The maximum recorded temperatures at the epidermis and dermis are 65 °C after 20 seconds, 55 °C after 35 seconds, and 45 °C after 50 seconds. While the temperature in the focal areas decreases rapidly, the overall tissue temperature remains relatively stable. Extended contact with cryogenic spray has the potential to significantly lower the overall skin temperature, risking tissue freezing at the application site and adjacent areas. Figure 12, the chart illustrates the proportion of the region above the 42 °C threshold [4]. At 20 °C, all epidermis cells surpassed the damage threshold, with a significant reduction in the epidermal area above the threshold occurring around 21 seconds, decreasing to nearly 30% within seconds. The dermal region follows suit, experiencing a decline a few seconds after the epidermis. The epidermis takes approximately 38 seconds to entirely exceed the threshold, while the dermis requires around 51 seconds.

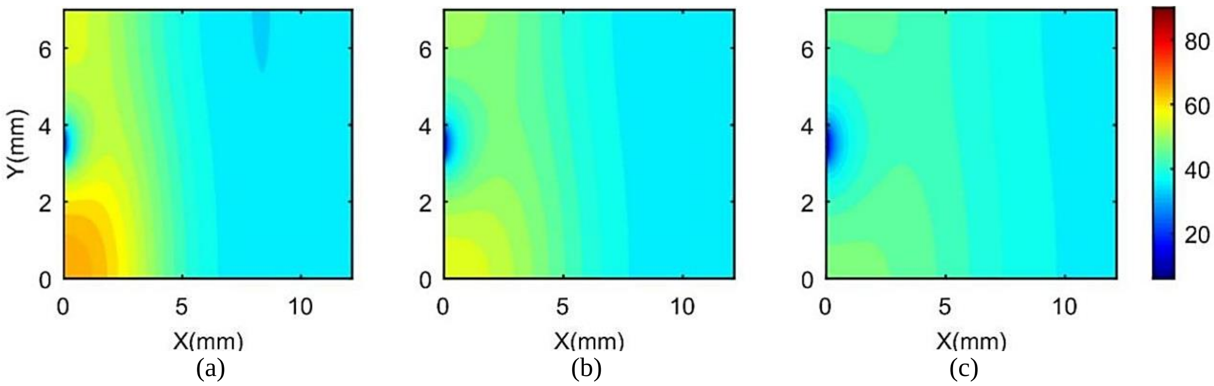

Figure 11. After burn tissue temperature during cryogenic cooling after: (a) 20 seconds, 35 seconds, and (c) 50 seconds

An observable trend shows an increase in adipose tissue temperatures reaching up to 45 °C, suggesting that cooling interventions have limited effect at this threshold. Furthermore, temperature elevations persist with heating, attributable to thermal conduction within the tissue, despite the application of a cooling agent. Beyond 45 seconds, the area above the threshold rises by almost 40%, contrasting with the 20% increase during cooling initiation, and nearly reaches 0% after approximately 58 seconds. In Figure 13, the chart depicts the area affected by first- and second-degree burns under cryogenic cooling. The epidermal area affected by first-degree burns increases from around 87% to 90% in about 28 seconds, while the dermal area reaches 100% after 50 seconds, starting from 81%. In fat tissues, slightly over 7% of the area is impacted by first-degree burns after 50 seconds, compared to just over 2% during the heating period. For second-degree burns, the epidermal region sees a nearly 3% increase from 84%, whereas the dermis experiences an increase from 76% to 81% after 50 seconds. Notably, the fat region exhibits the smallest increase in the percentage of the area affected by second-degree burns, rising from 1% to almost 4% after 50 seconds.

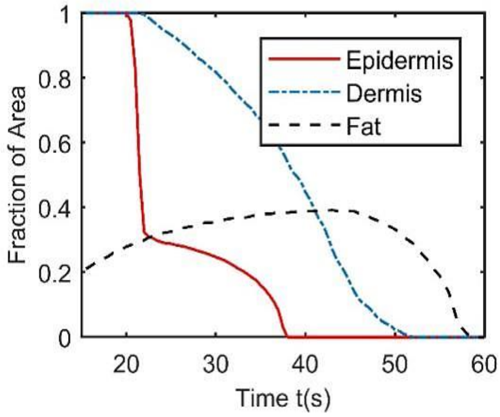

Figure 12. Fraction of area that undergoes damage threshold temperature during cryogenic cooling

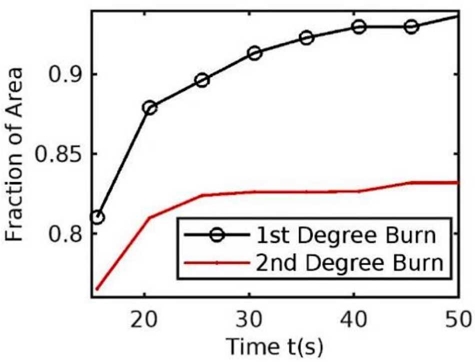

(a)

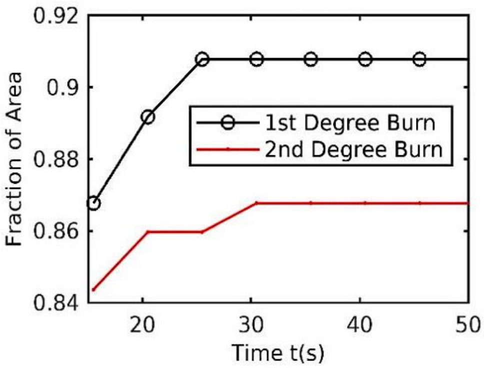

(b)

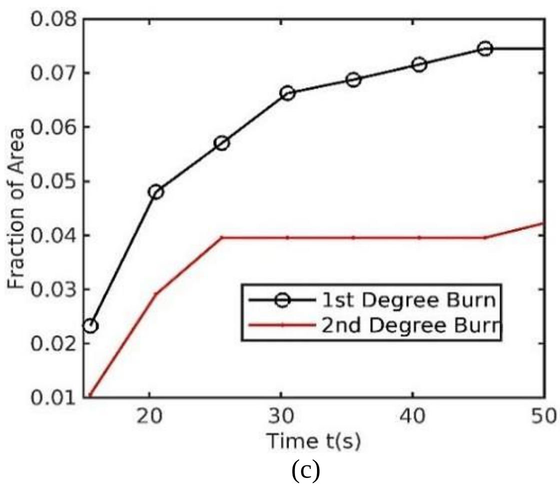

(c)

Figure 13. Fraction of Area affected by Burn during cryogenic cooling at: (a) epidermis, (b) dermis, and (c) fat

3.6 Cooling Efficacy

To determine the effectiveness of cooling, we assess the proportional decrease in the region affected by elevated temperatures or burns in comparison to the surrounding ambient air. The formula for calculating cooling efficacy is expressed as follows:

$$\epsilon(\%) = \frac{\Omega - \Omega_{amb}}{\Omega_{amb}} \times 100\% \tag{16}$$

In this equation, Ω represents the extent of damage or burns resulting from various cooling techniques, with reference to ambient air cooling. Figure 14, the effectiveness of cooling is illustrated concerning the damage threshold value, while Figures 3 and 4 present the cooling effectiveness from the perspectives of first- and second-degree burns. Across all three figures, it is evident that ice cooling demonstrates the highest efficacy, followed by flash water jet cooling and water bath cooling in the current experimental setup. Conversely, cryogenic cooling proves to be the least efficient method, primarily due to its limited skin surface exposure of only 8 mm, the lowest among the cooling techniques assessed. From the standpoint of damage threshold, ICE cooling achieves 100% cooling efficacy after approximately 32 seconds, while flush water cooling and water bath cooling reach the same level at 38 seconds and 42 seconds, respectively. In contrast, cryogenic cooling lags behind, achieving only approximately 52% efficiency after 65 seconds.

Examining the scenario from a first-degree burn perspective, ice cooling attains a maximum efficiency of 45% after 65 seconds. In comparison, flush water cooling, water bath cooling, and cryogenic cooling show maximum efficiencies of nearly 35%, 28%, and 24%, respectively. From a second-degree burn standpoint, ice cooling leads with an efficiency of almost 42%, followed by flush water cooling at nearly 25%, cryogenic cooling at 24%, and water bath cooling at 22% after 65 seconds. Considering both damage threshold and burn perspectives, the ice cooling method emerges as the most efficient in the current experimental setup. Convection cooling through cool water flush and water bath cooling exhibit comparable efficiency levels, with flush water cooling showing a slightly better outcome in terms of efficacy. On the other hand, cryogenic cooling consistently demonstrates the lowest level of efficiency when compared to the other cooling techniques assessed. Water immersion is effective for cooling superficial burns confined to the epidermis, whereas applying forced water jets offers enhanced cooling for deeper burns that extend into the dermis and subcutaneous fat.

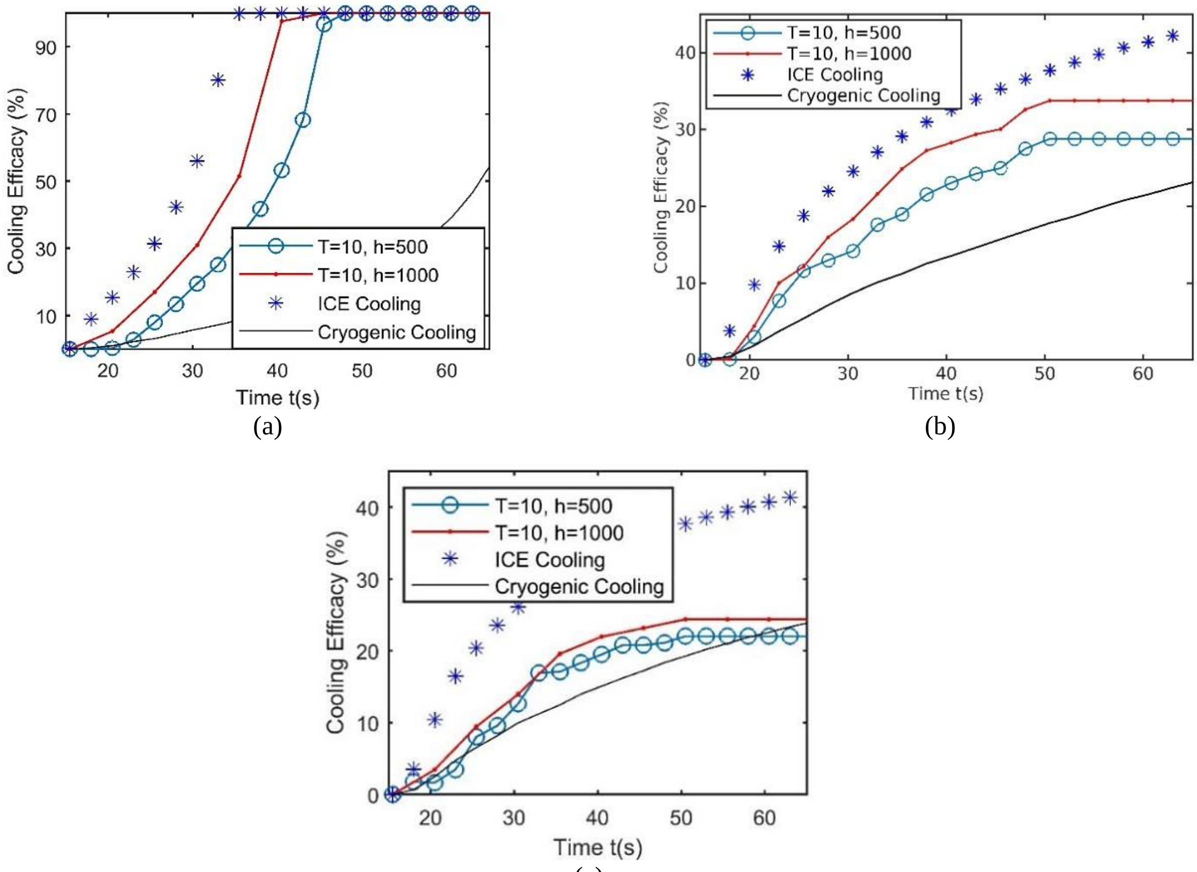

(a) (b) (c)

Figure 14. Cooling Efficacy from burn point of view: (a) damage threshold, (b) first degree burn, and (c) second degree burn

4. CONCLUSIONS

This study provides a detailed analysis of burn injuries and the impact of various cooling methods through a developed finite element model. Among the cooling strategies, forced convection cooling via a cold-water jet demonstrated the highest efficacy by reducing tissue temperatures below the critical threshold in just 32 seconds, compared to 45 seconds with water immersion. Notably, ice contact cooling achieved 100% cooling effectiveness based on the damage threshold but carried risks of hypothermia and tissue freezing, emphasizing the need for cautious application. The quantitative analysis reveals that, in forced water jet cooling, epidermal temperatures decreased to 30 °C within 50 seconds, compared to 45 °C in natural convection cooling under ambient air. Ice cooling was similarly effective but posed challenges due to uneven cooling between layers—dermal temperatures took longer to stabilize, dropping to 30 °C after 50 seconds. Cryogenic spray cooling, although initially promising with temperatures reaching 0°C within 50 seconds, proved the least effective overall due to limited surface exposure, achieving only 52% efficiency within 65 seconds. The prioritization of cooling techniques emphasizes that methods with higher heat transfer coefficients, such as flush water jets (1000 $W/m^2 \cdot K$), outperform traditional approaches. Future research should explore the long-term effects of these cooling methods on recovery and the development of optimized cooling applicators to reduce risks such as hypothermia.

ACKNOWLEDGEMENTS

We would like to acknowledge Shahajalal University of Science and Technology research center, Bangladesh for funding this research under grant number AS/2021/1/32.

CONFLICT OF INTEREST

The authors declare no conflicts of interest

AUTHORS CONTRIBUTION

A. M. M. Mukaddes (Conceptualization; Methodology; Review and editing; Supervision)
M. Sannyal (Model development; Coding; Visualization; Original draft)
M. Junaid (Resources; Writing; Visualization; Review and Editing)

AVAILABILITY OF DATA AND MATERIALS

The data supporting this study's findings are available on request from the corresponding author.

ETHICS STATEMENT

This research does require approval from any ethical board, as no experiment was done or no data was collected from human or animal.

REFFERENCE

[1] WHO, "Burns," World Health Organization [Online], 2023. Available: https://www.who.int/news-room/fact-sheets/detail/burns

[2] T. Zebra, "House Fire Statistics," The Nation Leading Independent Insurance Comparison Site [Online], 2023. Available: https://www.thezebra.com/resources/research/house-fire-statistics/

[3] W. Żwierełło, K. Piorun, M. Skórka-Majewicz, A. Maruszewska, J. Antoniewski, I. Gutowska, "Burns: classification, pathophysiology, and treatment: A review," *International Journal of Molecular Sciences*, vol. 24, no. 4, p. 3749, 2023.

[4] M. J. Simpson, S. McInerney, E. J. Carr, L. Cuttle, "Quantifying the efficacy of first aid treatments for burn injuries using mathematical modelling and in vivo porcine experiments," *Scientific Reports*, vol. 7, no. 1, p. 10925, 2017.

[5] J. P. Abraham, B. Plourde, L. Vallez, J. Stark, K. R. Diller, "Estimating the time and temperature relationship for causation of deep-partial thickness skin burns," *Burns*, vol. 41, no. 8, pp. 1741–1747, 2015.

[6] A. M. M. Mukaddes, M. Junaid, "Running water as first aid for burn and early hypothermia: A numerical investigation on human skin," *Burns Open*, vol. 8, no. 2, pp. 105–111, 2024.

[7] K. G. Klavuhn, D. Green, "Importance of cutaneous cooling during photothermal epilation: Theoretical and practical considerations," *Lasers in Surgery and Medicine*, vol. 31, no. 2, pp. 97–105, 2002.

[8] Y. Cao, T. H. Lei, F. Wang, B. Yang, T. Mündel, "Head, face and neck cooling as per-cooling (cooling during exercise) modalities to improve exercise performance in the heat: A narrative review and practical applications," *Sport Medicine*, vol. 8, no. 16, pp. 1-17, 2022.

[9] P. Smakulski, "Method of high heat flux removal by usage of liquid spray cooling," *Archives of Thermodynamics*, vol. 34, no. 3, pp. 173–184, 2013.

[10] E. A. Ahmed, S. Y. Mohammad, D. A. Abdelatief, A. S. Ali, "Effect of cryotherapy on pain associated with chest tube removal after thoracotomy," *Evidence-Based Nursing Research*, vol. 5, no. 3, pp. 22–35, 2023.

[11] M. Nizamoglu, A. Tan, T. Vickers, N. Segaren, D. Barnes, P. Dziewulski, "Cold burn injuries in the UK: The 11-year experience of a tertiary burns centre," *Burns Trauma*, vol. 4, no. 1, pp. 1-8, 2016.

[12] L. Cuttle, M. Kempf, P. Y. Liu, O. Kravchuk, R. M. Kimble, "The optimal duration and delay of first aid treatment for deep partial thickness burn injuries," *Burns*, vol. 36, no. 5, pp. 673–679, 2010.

[13] A. M. M. Mukaddes, R. Shioya, M. Ogino, D. Roy, R. Jaher, "Finite element-based analysis of bio-heat transfer in human skin burns and afterwards," *International Journal of Computational Methods*, vol. 18, no. 3, p. 2041010, 2021.

[14] A. G. Shulman, "Ice water as primary treatment of burns: simple method of emergency treatment of burns to alleviate pain, reduce sequelae, and hasten healing," *Jama*, vol. 173, no. 17, pp. 1916-1919, 1960.

[15] H. H. Pennes, "Analysis of tissue and arterial blood temperatures in the resting human forearm," *Journal of Applied Physiology*, vol. 1, no. 2, pp. 93-122, 1948.

[16] C. Kumari, A. Kumar, S. K. Sarangi, A. Thirugnanam, "Effects of spray parameters on skin tumour ablation volume during cryotherapy," *Australasian Physical and Engineering Sciences in Medicine*, vol. 42, no. 2, pp. 453–464, 2019.

[17] D. A. Torvi, J. D Dale, "A finite element model of skin subjected to a flash fire," *Journal of Biomechanical Engineering*, vol. 116, no. 3, pp. 250-255, 1994.

[18] F. Xu, T. J. Lu, K. A. Seffen, "Biothermomechanical behavior of skin tissue," *Acta Mechanica Sinica/Lixue Xuebao*, vol. 24, no. 1, pp. 1–23, 2008.

[19] S. Chakraverty, N. Mahato, P. Karunakar, T. Rao. Weighted Residual Methods. 1st Ed. Udicha, India: Wiley Telecom, 2019.

[20] M. Sannyal, A. M. M. Mukaddes, "Numerical investigation of tissue-temperature controlled system in thermal ablation: A finite element approach," *Journal of Applied and Computational Mechanics*, vol. 7, no. 3, pp. 1826–1835, 2021.

[21] H. G. Kumie, A. A. Tiruneh, G. A. Derese, "Crank–Nicolson method for solving time-fractional singularly perturbed delay partial differential equations," *Research in Mathematics*, vol. 11, no. 1, pp. 1-15, 2024.

[22] M. Jamil, E. Y. K. Ng, "To optimize the efficacy of bioheat transfer in capacitive hyperthermia: A physical perspective," *Journal Thermal Biology*, vol. 38, no. 5, pp. 272–279, 2013.

[23] J. Ma, X. Yang, Y. Sun, J. Yang, "Thermal damage in three-dimensional vivo bio-tissues induced by moving heat sources in laser therapy," *Scientific Reports*, vol. 9, no. 1, p.10987, 2019.